Title

ECG-free cine MRI with data-driven clustering of cardiac motion for quantification of ventricular function.

Journal

NMR in Biomedicine, 37(4)

Authors

Ming, Zhengyang
Pogosyan, Arutyun
Gao, Chang
et al.

Publication Date

2024-04-01

DOI

10.1002/nbm.5091

Peer reviewed

HHS Public Access

Author manuscript

NMR Biomed. Author manuscript; available in PMC 2025 April 01.

Published in final edited form as:

NMR Biomed. 2024 April ; 37(4): e5091. doi:10.1002/nbm.5091.

ECG-free cine MRI with data-driven clustering of cardiac motion for quantification of ventricular function

Zhengyang Ming, BS[1,2], **Arutyun Pogosyan, MD**[3], **Chang Gao, PhD**[1,2], **Caroline M. Colbert, PhD**[1,2,3], **Holden H. Wu, PhD**[1,2,4], **J. Paul Finn, MD**[1,2], **Dan Ruan, PhD**[1,4,5], **Peng Hu, PhD**[1,2,4], **Anthony G. Christodoulou, PhD**[4,6], **Kim-Lien Nguyen, MD**[1,2,3,4]

[1]Physics and Biology in Medicine Graduate Program, University of California, Los Angeles, CA, USA

[2]Department of Radiological Sciences, David Geffen School of Medicine at UCLA, CA, USA

[3]Division of Cardiology, David Geffen School of Medicine at UCLA and VA Greater Los Angeles Healthcare System, CA, USA

[4]Department of Bioengineering, University of California, Los Angeles, CA, USA

[5]Department of Radiation Oncology, David Geffen School of Medicine at UCLA, CA, USA

[6]Biomedical Imaging Research Institute, Cedars-Sinai Medical Center, Los Angeles, CA

Abstract

Background: Despite the widespread use of cine MRI for evaluation of cardiac function, existing real-time methods do not easily enable quantification of ventricular function. Moreover, segmented cine MRI assumes periodicity of cardiac motion. We aim to develop a self-gated, cine MRI acquisition scheme with data-driven cluster-based binning of cardiac motion.

Methods: A Cartesian golden-step balanced SSFP sequence with sorted k-space ordering was designed. Image data were acquired with breath-holding. Principal component analysis and k-means clustering were used for binning of cardiac phases. Cluster compactness in the time dimension was assessed using temporal variability and dispersion in the spatial dimension was assessed using the Calinski-Harabasz index. The proposed and the reference ECG-gated cine methods were compared using a 4-point image quality score, SNR and CNR values, and Bland-Altman analyses of ventricular function.

Results: A total of 10 subjects with sinus rhythm and 8 subjects with arrhythmias underwent cardiac MRI at 3.0T. The temporal variability was 45.6ms (cluster) vs 24.6ms (ECG-based) ($p < 0.001$), and the Calinski-Harabasz index was 59.1±9.1 (cluster) vs 22.0±7.1 (ECG-based) ($p < 0.001$). In subjects with sinus rhythm, 100% of the end-systolic and end-diastolic images from both the cluster and reference approach received the highest image quality score of 4. Relative to the reference cine images, the cluster-based multiphase (cine) image quality consistently received

Address correspondence to: Kim-Lien Nguyen, MD, David Geffen School of Medicine at UCLA, VA Greater Los Angeles Healthcare System, 11301 Wilshire Blvd, MC 111E, Los Angeles, CA 90073, Phone: 310.592.0386, Fax: 310.268.3258, klnguyen@ucla.edu.

The authors have no relevant conflict of interests.

a 1-point lower score ($p < 0.05$); whereas, the SNR and CNR values were not significantly different ($p = 0.20$). In cases with arrhythmias, 97.9% of the end-systolic and end-diastolic images from the cluster approach received an image quality score ≥ 3. The mean bias values for biventricular ejection fraction and volumes derived from the cluster approach vs reference cine were negligible.

Conclusion: ECG-free cine cardiac MRI with data-driven clustering for binning of cardiac motion is feasible and enables quantification of cardiac function.

Graphical Abstract

Real-time cine MRI methods do not easily enable quantification of ventricular function and conventional segmented cine MRI assume periodicity of cardiac motion. We showed that a Cartesian golden-step balanced steady-state free precession sequence with motion navigators can be used with k-means clustering to alleviate the dependency on periodic cardiac motion assumptions. The proposed approach produced images with good diagnostic quality and enabled quantitative evaluation of biventricular function for subjects in sinus rhythm and arrhythmias.

Keywords

cardiac motion; clustering; golden-step acquisition; self-gating; ECG-free; cine MRI

1. INTRODUCTION

Quantification of cardiac function and evaluation of morphology are crucial for diagnosis, therapeutic decisions, and prognostication of cardiovascular disease. Due to its superior blood-myocardium contrast, cine cardiac MRI using segmented balanced steady-state free precession (bSSFP) often serves as the reference method for quantification of cardiac function and morphology (1–3). This pulse sequence typically relies on an external electrocardiogram (ECG) signal to minimize cardiac motion artifacts and the MRI data are acquired over multiple heartbeats during breath-holding. Based on the ECG signal, k-space data acquired in the same cardiac phase over multiple heartbeats are combined and images from every cardiac phase are reconstructed respectively.

Despite the widespread use of 2D cine bSSFP in clinical cardiac MRI, reliance on ECG-gating to resolve cardiac motion has several disadvantages including the well-known magnetohydrodynamic effect, which can distort the ECG signal at magnet field strengths ≥3.0T (4). Although ECG-gating can be performed prospectively or retrospectively, prospective ECG triggering is sometimes used instead of retrospective gating to prevent false associations with ECG signal spikes other than the R wave. End-diastolic events, however, cannot be captured using prospective triggering. In practice, retrospective ECG gating is more commonly used because continuous acquisition ensures that all cardiac phases are captured, but both prospective and retrospective approaches have challenges when encountering arrhythmias and low amplitude R-wave. Minor irregularity of the R-R interval during image acquisition can also lead to significant artifacts (5).

Althought self-gating methods exist and were designed to mitigate ECG-dependency, current ECG- and self-gating approaches assume that cardiac motion is periodic with a well-defined and narrow range of frequencies (6–9). More specifically, self-gating extracts cardiac motion

signal from the acquired data by using band-pass filters (8) that focus on a fixed frequency range between 0.5–2.5Hz and assumes periodic cardiac motion within this range, which corresponds to an RR interval range of 400ms to 2000ms. Newer self-gating methods apply motion detection using pattern recognition strategies such as singular spectrum analysis (10) and independent component analysis (11) to alleviate the dependence on assumptions related to the periodicity of cardiac motion. However, quantification of ventricular ejection and volumes remain challenging in settings of non-periodic and complex cardiac motion.

For conventional cine MRI, strategies to handle irregular cardiac motion include arrhythmia rejection (12), prospective gating, beat-type gating (13), and real-time imaging. Arrhythmia rejection and beat-type gating, however, are not always consistently reliable in clinical practice. Arrhythmia rejection compares the R-R intervals to that of a predefined reference duration; if the R-R interval exceeds the predefined limit, the data from the extrasystolic and postextrasystolic beats are rejected. Incorrect acceptance of data from an ectopic beat can occur and corrupted data are incorporated into the reconstruction, which can result in image artifacts (14). Prospective gating can also improve the image quality in certain types of arrhythmias by capturing the beginning and end of systolic frames but at the sacrifice of incomplete capture of the end-diastolic phase. The beat-type gating method for cardiac motion management divides motion data into different types based on the morphology of the QRS complex and can cope with relatively regular arrhythmias such as bigeminy and trigeminy (13). All three methods rely on the ECG signal and are less able to handle rhythms that lack predictable patterns, or “irregularly irregular” rhythms. In contrast, real-time imaging strategies (15) and research methods that incorporate low-rank models (16) or compress sensing (17) can yield reasonable spatiotemporal resolution with fast acquisition in the setting of arrhythmias. In the setting of complex cardiac motion however, quantification of ejection fraction (EF) and volumes using real time remain clinically challenging. The vast number of acquired images cannot be handled by commercially available post-processing software to yield clinically meaningful quantitative metrics of cardiac function (18–20).

Given the clinical importance of quantitative functional metrics in cardiac cine MRI and the aforementioned challenges, we propose an ECG-free, 2D cine acquisition and clustering scheme for binning of cardiac motion. The acquisition uses a modified version of the Cartesian golden-step (21) bSSFP pulse sequence (22) with sorted k-space ordering to mitigate bSSFP eddy current effects and motion navigators to eliminate ECG dependency. We aim to provide early evidence for a universal cardiac binning strategy that makes no assumptions about the periodicity or frequency range of cardiac motion states for sinus rhythm and arrhythmias.

2. METHODS

This study was approved by our local Institutional Review Board and all subjects provided written informed consent. An overview of the proposed framework for image acquisition, data-driven cluster-based motion binning, and image reconstruction using an eigenvalue approach to auto-calibrating parallel MRI (ESPIRiT) (23) is presented in Figure 1.

2.1 Pulse Sequence

A free-running Cartesian sequence with sorted golden-step trajectory (24) and bSSFP readout was used (Figure 2). We chose a bSSFP readout because of its intrinsic high blood-myocardium contrast and its widespread clinical use. ECG signal was simultaneously recorded to support the reference ECG-based reconstruction. Relative to the conventional golden-step pulse sequence (21), the sorted golden-step phase encoding scheme was designed to (a) promote adequate k-space coverage within clustered cardiac bins and (b) to mitigate severe eddy current artifacts. The locations of k-space line before sorting follows the golden step method, represented as Eq 1.

$$PE_i = mod(PE_{i-1} + F_{small},\ F_{large}) \quad \text{(Eq 1)}$$

PE_i is the location of the ith phase encoding line ranging from 1 to the maximum number of phase encoding N_{PE}. F_{small} is the largest Fibonacci number smaller than N_{PE}. F_{large} is the smallest Fibonacci number larger than N_{PE}. For example, if $N_{PE} = 192$, then $F_{small} = 144$ and $F_{large} = 233$. Mod(x, y) represents the remainder when x is divided by y. The phase encoding schedule generated by Eq 1 was then reordered by dividing the schedule into fixed temporal segments (in this work, 20 lines per segment) and sorting the phase-encodes within each segment (Figure 2).

Extra k-space center lines were added after every n^{th} TR to act as motion navigators for the purpose of obtaining information about mechanical cardiac motion. These navigator lines serve as the source for the motion matrix **X** used in the subsequent clustering of motion data. Thus, each data frame consisted of the four k-space lines, and the corresponding navigator line is considered to have the same motion state as the data frame. With $n = 4$, the corresponding temporal resolution of the navigators was 3.4 * (4+1) = 17 ms. Although the additional k-space center lines were needed for motion binning, the additional lines may contribute to image artifacts due to rapid gradient changes.

2.2 Navigator Data Processing, Motion Data Binning, and Image Reconstruction

Unlike conventional self-gating strategies, the proposed technique uses a clustering algorithm for binning of mechanical cardiac motion. After acquiring the additional k-space center lines as motion navigators (henceforth known as motion navigator data), data from these k-space center lines were converted to 1D projections in image space using inverse Fast Fourier Transform (iFFT) and concatenated to form a motion matrix **X**. Matrix **X** represents the time series of self-gating projections into image space. A sample illustration of navigator data in image space before and after clustering is shown in Figure 3. The dimension of matrix **X** is $N_{\text{coil}} \times M \times T$, where M represents the number of frequency encoding points, N_{coil} represents the number of coils, and T represents the number of navigators along the time dimension. The typical value of N_{coil} ranged from 2 to 4. Based on the magnitude of the coil sensitivity maps, data from the coil elements closest to the heart were chosen manually to improve the capturing of mechanical cardiac motion.

Next, the spatial gradient of the projections was computed. Principal component analysis (PCA) using singular value decomposition (SVD) of the spatial gradient matrix identified the 20 largest principal components and generated a compressed matrix X', which was used as the input into the cluster algorithm. The PCA in this work reduces only the spatial dimension, such that X' maintains the same temporal dimension with X. Next, a k-means clustering algorithm (25) was performed on X' to bin the acquired data into cardiac phases. The k-means algorithm achieved this purpose by evaluating similarity of motion information from different navigator lines and assigning cluster membership based on motion states. Navigator lines in the same cluster were considered to have similar motion. The clustering algorithm, based on motion information from the navigator lines, generated the cluster membership of the navigator lines. Cluster membership information of the navigator lines was later used in the image reconstruction step whereby k-space center lines corresponding to the navigator lines in the same cluster are binned together. To mitigate the effect of randomness for initial conditions, the k-means algorithm was repeated 100 times with random initial values until a stable solution was achieved. The cluster assignments, which minimized the sum of in-cluster distances among all the clusters, were used for data binning. We chose 25 clusters to yield a temporal resolution <40ms, which is typically used in clinical imaging. To prevent certain clusters from having too few data points, we computed the cluster size ratio between the cluster with the fewest data points and the cluster with the most data points. If the ratio were less than 15%, the algorithm would be repeated until the ratio is ≥15%. If the ratio were <15% for 10 times out of the 100 repetitions, the solution with the largest ratio among the 10 stable solutions was chosen.

Data within each cluster were assumed to represent one cardiac phase. The ESPIRiT reconstruction method was applied to every cluster bin to generate cine images. When multiple data points from the same k-space location were binned into the same cluster, the algorithm retained only the data with the smallest distance to the centroid of the cluster. Although some data points were further from the centroids of the clusters than others, we did not discard the outliers. Every data point was used for binning and reconstruction.

To generate a cine video based on the images from each cluster bin, the temporal order of the phases was established using two different strategies: one for sinus rhythm and one for the select cases of arrhythmias. For sinus rhythm, the temporal order was generated based on the recorded ECG. The temporal distances of data relative to the R wave were used to represent temporal locations in the cardiac cycle. Based on the average values of the temporal locations for the data in each motion cluster, temporal ordering was established. For select arrhythmia cases, the temporal order was generated based on the natural sequential time stamp of the acquired navigator data, i.e. images with a shorter (lower) time stamp are ordered earlier and images with a longer (larger) time stamp, are ordered later in the cardiac cycle.

SVD, clustering, and ESPIRiT were implemented using MATLAB version 2021a (MathWorks, Natick, MA, USA). ESPIRiT reconstruction (26) was customized to fill the k-space data using motion binning. Both k-means clustering analysis for motion binning and image reconstruction were performed offline.

2.3 Image Acquisition

With approval from the local Institutional Review Board and in compliance with the Health Insurance Portability and Accountability Act, this study recruited 18 subjects to undergo cardiac MRI (sinus rhythm, n=10; arrhythmias, n=8 [n=3 premature ventricular contractions, n=4 atrial fibrillation, n=1 premature atrial contractions). All imaging was performed on a 3.0T clinical scanner (Skyra; Siemens Healthcare, Erlangen, Germany) equipped with an 18-channel phased-array body coil. Representative scan parameters are shown in Table 1. Images were acquired using both our proposed pulse sequence and the conventional ECG-gated segmented bSSFP cine sequence; the latter served as our reference in subjects with sinus rhythm. In the patients with atrial fibrillation, real-time cine cardiac MR served as reference (Table 1). Although our proposed sequence does not require breath-holding, the images were acquired with breath-holding (~18s) to enable better comparison with reference methods, which required breath-holding. The ECG signal was simultaneously recorded for use as a reference to evaluate retrospective data clustering and for ECG-based image reconstruction, which henceforth, will be referred to as ECG-based.

2.4 Analysis of Cluster Algorithm Performance

The performance of the cluster algorithm was evaluated using several metrics: 1) quality of data cluster selection, 2) dispersion of motion data clusters in the time dimension using temporal variability, and 3) overall cluster performance based on the Calinski-Harabasz index (23). To evaluate the quality of data cluster selection after binning, we computed the number of data points in each cluster and the percent of k-space lines that were filled for every cardiac phase. In the cardiac motion dimension, the temporal distance between motion data clusters and the start of every heartbeat was evaluated by computing the intervals between the navigator data and the R-wave from the simultaneously recorded ECG. These intervals describe the locations of the navigator data within the cardiac cycle.

To determine the cluster compactness and inter-cluster distance in the time dimension as a reflection of pairwise matching between cluster membership and cardiac phase, the SD of the time intervals for each cluster within the cardiac cycle was computed, and will be referred to as temporal variability (see Supplementary Material). Temporal variability has been used to evaluate the consistency between self-gating and ECG triggering (27). In the current work, temporal variability represents how widely the cluster spreads in the time dimension and the temporal consistency between cluster distribution and the simultaneously recorded ECG signal. In brief, data points within a cluster were from different heartbeats and their temporal locations within the cardiac cycle were calculated as the temporal distance from the R-wave. A smaller temporal variability means the temporal locations are closer to each other and reflects a denser cluster distribution in the time dimension and therefore, better consistency with the ECG signal. The average temporal variability for both the cluster-based and ECG-based reconstructions for all subjects was computed and the average temporal variability for the ECG-based reconstruction was used as reference.

To directly evaluate cluster performance in the spatial dimension, the Calinski-Harabasz index (28) was calculated (see Supplementary Material). The Calinski-Harabasz index, also known as the variance ratio criterion, reflects the ratio between the sum of inter-

cluster dispersion and the sum of intra-cluster dispersion for all clusters. A higher Calinski-Harabasz index value describes clusters that are dense and well separated. The Calinski-Harabasz index for the cluster-based method was calculated using the PCA-processed navigator data and the clustering solution derived from the clustering algorithm. The Calinski-Harabasz index for the ECG-based method was used as a reference.

2.5 Analysis of Image Quality

The image quality and several quantitative metrics of cardiac function derived from the cluster-based and the standard reference method were evaluated. Two CMR readers (KLN, >10 years of cardiac MR experience; AP, one year of cardiac MR experience) graded the image quality in consensus using a 4-point Likert scale (Supplemental Material, Additional Table S1). Images from the reference ECG-gated segmented cine bSSFP method (subjects with sinus rhythm subjects) and the reference real-time bSSFP method (subjects with arrhythmias), ECG-free cluster-based sorted golden-step reconstruction, and ECG-based sorted golden-step reconstruction, were randomized and shown to both readers, who were blinded to the reconstruction method. Single phase end-systolic and end-diastolic images from the ventricular base, mid, and apical slice from all subjects were scored first because the systolic and diastolic frames are most important for cardiac function analysis. Multiphase images of the ventricular base, mid, and apical slice from sinus rhythm subjects were then scored in cine mode.

Regions of interest (ROIs) were placed within the mid-ventricular blood pool, myocardium, and air (outside the imaged body but within the field of view). Mean signal intensity (SI) was recorded in blood and myocardium, and the standard deviation (SD) of the SI was recorded in air to quantify image noise. The signal-to-noise ratio (SNR) of all tissue types was calculated as: $\mathrm{SNR} = \frac{\mathrm{mean}(\mathrm{SI}_{\mathrm{tissue}})}{\mathrm{SD}(\mathrm{SI}_{\mathrm{air}})}$, where $\mathrm{SD} = \text{standard deviation}$.

The contrast-to-noise ratio (CNR) between blood and myocardium was computed as: $\mathrm{CNR} = (\mathrm{SI}_{\mathrm{blood}} - \mathrm{SI}_{\mathrm{myocardium}})/\mathrm{SD}(\mathrm{SI}_{\mathrm{air}})$. To quantitatively assess the impact of clustering on image noise, we computed the ratios of the SNR between the cluster-based and the ECG-based reconstruction as well as the ratios of the CNR between the two methods:

$$ratio_{\mathrm{SNR}} = \frac{SNR_{cluster}}{SNR_{ECG\ gating}} \quad \text{(Eq 2)}$$

$$ratio_{\mathrm{CNR}} = \frac{CNR_{cluster}}{CNR_{ECG\ gating}} \quad \text{(Eq 3)}$$

Using commercially available software (cvi42, Circle Cardiovascular Imaging, Calgary, AB, Canada), we quantified the right and left ventricular (RV/LV) ejection fraction (EF), end-diastolic volume (EDV), end-systolic volume (ESV), and LV mass for both the cluster-based and reference cine or real-time images using a full stack of the ventricular short-axis images. To quantify biventricular function using real-time images of patients with arrhythmias, we

derived the ventricular volumes and EFs by averaging diastolic and systolic values across three consecutive heartbeats.

2.6 Statistical analysis

Statistical analysis was performed using MATLAB version 2021a (MathWorks, Natick, MA, USA). Continuous variables are summarized as mean±SD or median and interquartile range (IQR) as appropriate. Categorical variables are summarized as frequencies or percentages where appropriate. The Kolmogorov-Smirnov test was used to test the normality of the data. For group comparisons, a two-tailed paired sample t-test was performed on normally distributed data. For non-parametric image quality score comparisons of repeated measures (reference segmented bSSFP method, cluster-based sorted golden-step reconstruction, and ECG-based sorted golden-step reconstruction), the Friedman test was performed for multiple groups comparison, followed by post-hoc group analysis using Tukey's test. Wilcoxon rank sum test was performed on two group comparisons. Bland-Altman analyses were performed to assess the bias for biventricular EF, EDV, and ESV values derived from the cluster-based reconstruction and the reference bSSFP cine images or the reference real-time images. Coefficients of variation (CV) were derived from Bland-Altman analysis. A p value of < 0.05 was considered statistically significant.

3. RESULTS

A total of 18 volunteers and patients (53.8±18.1 years, n=8 females) underwent imaging at 3.0T. All subjects were included in the validation of ventricular EF, volume, and mass. The heart rate was 62±15 bpm. The reported 24-hour PVC burden of the three PVC subjects were 36.8%, 17.0% and 8.9%, respectively. The PVC burdens of the PVC patients during the scan were 37.5%, 15.6% and 31.3%. The PAC burden of the PAC patient during the scan was 14.3%. The patients with atrial fibrillation were in constant atrial fibrillation throughout the scan.

3.1. Performance of cluster-based data binning

Relative to higher principal components, we found the intrinsic nature of PCA to favor lower principal components for discrimination between motion states and effective binning of cardiac motion (Figure 4). The clusters on average contained 52±24 data points, and 62.0%±19.3% of k-space data of the clusters were filled. Based on data distribution in the time dimension, the temporal variability for the cluster-based and the reference ECG-gating methods were 45.6ms and 24.6ms ($p < 0.001$), respectively. A higher temporal variability for the cluster-based method was observed and the cluster-based method had greater data distribution in the time dimension relative to ECG-gating. The Calinski-Harabasz index for the cluster- and ECG-based methods were 59.1±9.1 vs 22.0±7.1 ($p < 0.001$). Relative to the ECG-based method, the significantly higher Calinski-Harabasz index for the cluster-based method suggests better performance of the proposed clustering algorithm in the spatial dimension. Figure 5 shows a comparison of data distribution between the cluster- and the ECG-based method in the time dimension. Data at end diastole and early systole phase are shown. Relative to the time stamp data distribution from the ECG-based method, the data distribution from the cluster method has wider temporal distribution. The observed

difference is likely related to preferential use of spatial similarity in the cluster method; whereas, the ECG-based method directly used the time information from the recorded ECG. Figure S1 (Supplemental Material) shows the data distribution of RR intervals for every cluster in one dataset belonging to a patient in sinus rhythm with a heart rate of 60 bpm. Clusters with higher outliers will increase the temporal variability. Although clusters 12 and 13 have the most outliers (6.25% and 5.43%, respectively) and did not have a large effect on the image quality, the outliers do occasionally lead to ambiguity for data points at end-diastole and the beginning of early systole.

3.2 Image Quality

The end-systolic and end-diastolic single-phase images generated by the cluster-based approach had no significant image artifacts. In subjects with sinus rhythm, a maximum single-phase image quality score of 4 was achieved by all three methods (cluster-based sorted golden-step reconstruction, ECG-based sorted golden-step reconstruction, and the reference segmented cine bSSFP) ($p = 0.38$). Figure 6 shows an example of short- and long-axis images acquired in a healthy volunteer using the proposed and the reference bSSFP sequence. Short-axis images from select phases of the cardiac cycle using the proposed and the reference methods demonstrate excellent image quality (Figure 7). The cine video had flickering artifacts that resulted in a lower overall multiphase image quality score compared to the reference method (see Supplementary Material Video S1). However, the flickering artifacts did not degrade sharpness of the cardiac borders and morphology.

Multiphase cine images using the cluster-based method received a score of ≥3 in 86.7% of cases whereas images from the ECG-based method received a score of ≥3 in 93.3% cases. The reference bSSFP method received a score of ≥3 in 100.0% of cases. The Friedman test showed there were significant differences in the multiphase image quality scores among the three methods ($p < 0.001$). Although there were significant differences between the reference bSSFP and the cluster-based method ($p<0.001$) as well as between the reference bSSFP and the ECG-based method ($p<0.001$), we found no significant difference between multiphase image quality scores of the cluster-based method and those of the ECG-based approach ($p=0.997$). In subjects with arrhythmias, diastolic and systolic images from reference real-time sequence received a score of ≥3 in 91.7% cases whereas images from the cluster-based method received a score of ≥3 in 97.9% cases. The Wilcoxon rank sum test showed there was no significant difference between the cluster-based method and reference real-time ($p=0.996$). Figure 8 shows sample images from a patient with PVCs (HR range 40–60 bpm) and a patient with atrial fibrillation (heart rate range 85–140 bpm). For the patient with atrial fibrillation, the commercially available real-time Cartesian bSSFP sequence was performed as reference. As depicted in Figure 8A, the cluster-based method was effective at generating single-phase systolic and diastolic images with little artifact in both settings of arrhythmia. Figure 8B shows a comparison of the simultaneously recorded ECG signal along with data points that were chosen for the corresponding early systolic and end-diastolic phase in the setting of sinus rhythm, PVC, and atrial fibrillation. The cluster-based method consistently identified the points immediately before the R peak for one cluster and the points immediately after the R peak for another cluster regardless of differences in the

QRS shape. This algorithmic behavior suggests the potential for differentiating motion states between data clusters.

The ratio of the cluster-based reconstruction SNR to that of the ECG-based SNR was 1.01±0.10. The ratio of the cluster-based reconstruction CNR to that of the ECG-based CNR was 1.04±0.10. Paired t-tests found no significant difference in the SNR and CNR values for the cluster-based vs the ECG-based method (SNR, p=0.38; CNR, p=0.16).

3.3 Quantitative Metrics of Biventricular Function

Paired t-tests found no significant difference between the reference method and the cluster-based reconstruction for quantification of LVEF, LV EDV, LV ESV, LV mass, RVEF, RV EDV, and RV ESV (Table 2). Bland-Altman analyses of EF, ventricular volumes, and LV mass derived from the cluster-based and reference bSSFP cine images of patients in sinus rhythm showed narrow limits of agreement, clinically negligible mean bias values, and CVs <5% for quantification of EF, ventricular volumes, and LV mass (Figure 9, Table 2). All data points were within the 95% limits of agreement. Correlation plots of these metrics also show $R^2 \geq 0.95$ (see Supplemental Material, Additional Figure S2). In the 10 subjects with sinus rhythm, LV EF was 57.9% ± 14.6% (reference) vs 57.5% ± 15.7% (cluster-based), RV EF was 53.2% ± 10.4% (reference) vs 52.7% ± 11.2% (cluster-based). In the 8 subjects with arrhythmias, LV EF was 28.7% ± 10.8% (reference) vs 27.8% ± 11.8% (cluster-based), and RV EF was 29.4% ± 14.2% (reference) vs 30.0% ± 14.5% (cluster-based).

4. DISCUSSION

Cine cardiac MRI using breath-held 2D-multislice bSSFP is the reference standard for clinical assessment of cardiac function and morphology. However, cine bSSFP is primarily dependent on ECG-gating, and alternative self-gating approaches rely on assumptions about periodic cardiac motion within a specific frequency range, which may not be applicable to all patients. We proposed a free-running segmented golden-step Cartesian sequence with sorted k-space ordering and motion navigators along with a cluster-based data binning approach. Compared to conventional ECG-gated cine bSSFP, there was no significant difference in the single-phase systolic and diastolic image quality achieved by the proposed approach, where both good qualitative and quantitative agreements were observed. Significant differences in multiphase image quality scores were noted among cluster-based, ECG-based, and the reference segmented cine bSSFP. However, all images were of diagnostic quality and more importantly, the mean bias between the proposed cluster-based and the reference segmented bSSFP methods for derivation of quantitative cardiac functional metrics (EF, volumes, mass) was negligible. These findings are hypothesis-generating and support the early feasibility of using a data-driven clustering approach to distinguish mechanical cardiac motion states in dynamic cardiac MRI. Once further developed, there is potential for using our cluster-based approach to enable quantification of cardiac function in settings of complex cardiac motion.

The novelty of our proposed workflow lies in removal of ECG signal reliance for gating, and lack of assumptions about cardiac motion periodicity or frequency pattern. Relative to images reconstructed using simultaneously recorded ECG, images derived from the

cluster-based method had no significant difference in SNR/CNR values, which is important for many commercial image processing software packages that rely on algorithms for semi-automated or automated image segmentation and quantification of cardiac function. Although the cluster-based technique did not use ECG gating, typical filtering, or correlation strategies employed by other self-gating methods (6–9), the images derived from the proposed cluster-based approach have comparable single-phase image quality as those from the ECG-gated reconstruction. The mean bias between the cluster-based and the reference cine bSSFP method for quantification of biventricular EF, volumes, and LV mass were small. The slightly higher CVs for RV functional metrics are likely related to greater sensitivity to through-slice motion and minor differences in subjective determination of inclusion or exclusion of the basal slice for RV metric quantification. It should be noted that the proposed sorted golden-step acquisition reflects a combination of the pure golden-step method and linear ordering. Relative to the pure golden-step method, the sorted golden-step acquisition reduces wide gaps between each step but increases the probability of overlapping k-space phase encoding after data binning compared with pure golden step. The increase in phase encoding overlap, however, is generally not significant.

From the standpoint of SNR and CNR, the cluster-based method performed similarly to ECG-gating. The SNR and CNR of the cluster-based method were higher than that of the ECG-based method because the cluster-based method generally bins more data into the diastolic and systolic phases than other phases. The major drawback from cardiac phases of nonuniform duration is for those cardiac phases with very short duration, there may be insufficient data for image reconstruction. Based on the current small dataset, mean bias values for volumetric quantification between the proposed and reference methods were negligible. We speculate that unlike the standard ECG-gating method which evenly distributes data into phase bins, the cluster-based method enhances the SNR/CNR by including more data in certain phases, but may do so at the expense of the other cardiac phases. This is acceptable in our applications for EF calculation because (a) the EF is a desired metric that is used clinically as a determinant for many therapeutic options, and (b) the EF is calculated based on the mechanical definitions of diastolic and systolic phases. For arrhythmias, this is also preferable because the clustering algorithm bins more data with consistent motion into the systolic and diastolic phases based on mechanical motion states, which may reduce artifacts and enhance image quality. The preliminary data in patients with PVC, PACs and atrial fibrillation highlight this potential, but detailed study in a larger patient cohort with arrhythmias will be needed.

In subjects with regular cardiac motion, there may be no clear preference between cluster-based method and ECG-gating methods. In contrast, for subjects with irregular cardiac motion, the different motion states for each heartbeat may vary and ECG-gating may lead to image artifacts because the latter assumes periodic cardiac motion in the time dimension. The cluster-based method can generate images with less cardiac motion related artifact because it naturally bins the data with consistent mechanical cardiac motion states together and apply them to irregular cardiac motion states without assuming regularity or periodicity of motion.

Although the single-phase image quality scores were not significantly different between the proposed and the reference methods, the multiphase image quality scores were significantly different. One reason for the difference in the multiphase image quality scores is the inserted navigator lines may have caused flickering artifacts seen on certain phases during cine (video) mode, which did not occur at end-systolic or end-diastolic frames. Even though the sorted golden step pulse sequence design was used to reduce eddy current artifacts, insertion of navigator lines at k-space center lines may result in sufficiently large gradient jumps between the image phase encoding gradient and gradient of the navigator. Because the navigator lines were inserted every 4 TR, the locations of their previously acquired line were different. Jumping back from different previously acquired lines may result in different eddy current artifacts. When images are played in a cine mode, the differences of these artifacts could be more obvious in the temporal dimension and cause flickering artifacts. We speculate the flickering artifact can be reduced by inserting the navigator less frequently or by applying a reconstruction strategy with a temporal total variation term along the cardiac phases (29). The second reason for the flickering artifact may be due to temporal inconsistency whereby the cluster-based method did not infer that data from adjacent time frames are more likely to be binned into the same or adjacent phase. This latter assumption is inherent in ECG gating.

The approach in this work differs from several methods that have been proposed in the literature. Compared to recent work on pseudo-projection motion tracking with sorted golden-step phase encoding (24), the proposed approach focuses on a non-ECG-gated strategy for dynamic cine image acquisition and development of a cluster-based data binning approach that uses existing motion to represent cardiac motion states. In (24), motion signal was indirectly acquired using pseudo-projection from near-center k-space data and the real temporal resolution of the acquired motion signal was limited by how often the Cartesian k-space trajectory was at near-center k-space. In contrast, the additional k-space center lines in our work were added to directly mark the motion signal, which increased the total scan time by 25%. This tradeoff was necessary for recording the direct motion signal in order to validate the proposed clustering algorithm; using the indirect method in (24) may confound this validation. If we used the same pseudo-projection strategy as (24), the effective temporal resolution of the motion signal would be ~40 ms. The temporal resolution therefore would be insufficient for patients with heart rates >60 bpm.

Cluster-based data binning has also been used in the similarity-driven multidimensional binning algorithm (SIMBA) for reconstruction of free-running, 3D radial, whole-heart magnetic resonance angiography (MRA) (30). The SIMBA method ascertains motion-suppressed data from the most populated or largest cluster (phase) rather than from all the clusters (phases). In doing so, the SIMBA method empirically assumes a tradeoff between explanatory capability and reduction of dimensionality such that 20 principal components sufficiently represent low-dimensionality data matrix and, based on prior knowledge derived from published work on triggered 3D radial coronary MRA, the number of k-clusters necessary for reconstruction of a whole-heart volume with isotropic spatial resolution. One of the main objectives of the SIMBA method was sharp depiction of the myocardium and coronary vasculature from a single cardiac phase, which is generally sufficient for routine MRA. For dynamic cine cardiac MR, we need both the end-systolic and the end-diastolic

phase for quantification of cardiac function. Thus, the cost function of the clustering algorithm varied based on the multiphase requirement. Lastly, the SIMBA method applied navigators in the superior-inferior direction to acquire motion signal, whereas the proposed work applied in-plane navigators.

Real-time cine MRI (31) has also been used clinically for depiction of cardiac function in patients with irregular heart rhythm who are able to breath-hold or in those who have sinus rhythm but are unable to breath-hold. Whereas the proposed method relies on motion similarity between data groups that are determined by the clustering algorithm, real-time imaging reconstructs images using k-space data from adjacent time frames by assuming that data from adjacent time frames belong to the same cardiac phase. In the example of a patient with atrial fibrillation, the proposed approach is robust to image artifacts at end-systole and end-diastole and has increased endocardial border edge-sharpness when compared to the reference real-time images. Despite advances in current state-of-the-art, commercially available implementation of real-time, the quantitative computation of biventricular function remains challenging.

Limitations

This study has several limitations. First, the subject cohort was relatively small, had a narrow range of heart rates, and was predominantly in sinus rhythm. However, the preliminary results are promising for patients in sinus rhythm and show early potential in select cases of arrhythmias. The results from k-means clustering are hypothesis generating, and support further optimization to enable direct cardiac phase assignment based on mechanical motion. Second, there were occasional outliers at end-diastole and at the beginning of early systole that resulted in ambiguity of cluster assignment, but the low percentage of cluster outliers did not have a large effect on the overall image quality. Moreover, we used the recorded ECG signal to calculate the interval between the data frame and the nearest R wave of the clusters and then ordered the images based on the average intervals. No temporal adjacency information from the recorded ECG signal or the total-time stamp of the system was applied. We speculate that adding a temporal continuity regularization term will both resolve the ambiguous temporal data points and help to improve cluster reordering. Third, to directly obtain motion information about the heart, we inserted additional k-space center line as navigators. This approach prolonged the image acquisition time by 25% (roughly ~3.5 secs). Although the total acquisition time was 18sec, the sequence does not require ECG triggering and can be performed without breath-holding. We also did not apply advanced acceleration strategies in our sequence. Future work can employ state-of-the-art acceleration methods to reduce the total acquisition time. In the current work, images were obtained under breath-held conditions to facilitate comparisons with the reference breath-held methods. Further modifications to facilitate free-breathing acquisitions would be helpful. Lastly, the insertion of navigator lines may contribute to additional eddy current artifacts or noise. Although we minimized the gaps between the navigator lines, residual effects remain present on the video representation and reflected as flickering artifacts. This is a major drawback and led to lower multi-phase image quality scores even though the flickering did not degrade the single end-diastolic and end-systolic images used for quantification of the ventricular EF and volumes. In future work, the effects of the navigator lines may be minimized by

incorporating filter-based methods at near-center k-space data to acquire simulated center k-space lines as navigator data (24). The location of the navigator lines can also be optimized to further reduce the gradient jumps.

5. CONCLUSION

An ECG-free data-driven cluster approach to discriminate and bin cardiac motion is feasible and enables quantitative evaluation of biventricular function. Good quality end-diastolic and end systolic images can be generated in sinus rhythm and in select cases of arrythmias. If successfully tested and optimized in a larger patient cohort with a wide spectrum of heart rate and rhythm, cluster-based cardiac motion management may provide a clinically suitable method for quantification of ventricular function in patients with complex arrhythmias.

Supplementary Material

Refer to Web version on PubMed Central for supplementary material.

ACKNOWLEDGEMENTS

The authors thank cardiovascular MRI technologists from the VA Greater Los Angeles Healthcare System and the Diagnostic Cardiovascular Imaging Section of the Department of Radiology at the David Geffen School of Medicine at UCLA. The views expressed in this article are those of the authors and do not necessarily reflect the position or policy of the Department of Veterans Affairs or the United States government. This work was supported by the National Institutes of Health (R01HL148182, R01HL127153) and the Veterans Health Administration (I01CX001901).

Availability of data and materials:

The datasets used and/or analyzed during the current study are available from the corresponding author on reasonable request.

Abbreviations

bSSFP	Balanced steady-state free precession
BPM	Beat per minute
CNR	Contrast to noise ratio
EDV	End-diastolic volume
EF	Ejection fraction
ESV	End-systolic volume
LV	Left ventricle
MR	Magnetic resonance
PCA	Principal component analysis
AF	Atrial fibrillation

PVC	Premature ventricular contraction
PAC	Premature atrial contraction
RV	Right ventricle
SAX	Short axis
SNR	Signal to noise ratio
TE	Echo time
TR	Repetition time

References

1. Carr JC, Simonetti O, Bundy J, Li D, Pereles S, Finn JP. Cine MR angiography of the heart with segmented true fast imaging with steady-state precession. Radiology. 2001;219(3):828–834. [PubMed: 11376278]
2. Longmore D, Underwood S, Hounsfield G, et al. Dimensional accuracy of magnetic resonance in studies of the heart. The Lancet. 1985;325(8442):1360–1362.
3. Sechtem U, Pflugfelder PW, Gould RG, Cassidy MM, Higgins CB. Measurement of right and left ventricular volumes in healthy individuals with cine MR imaging. Radiology. 1987;163(3):697–702. [PubMed: 3575717]
4. Felblinger J, Lehmann C, Boesch C. Electrocardiogram acquisition during MR examinations for patient monitoring and sequence triggering. Magnetic Resonance in Medicine. 1994;32(4):523–529. [PubMed: 7997120]
5. Bilchick KC, Berger RD. Heart rate variability. Journal of cardiovascular electrophysiology. 2006;17(6):691–694. [PubMed: 16836727]
6. Feng L, Axel L, Chandarana H, Block KT, Sodickson DK, Otazo R. XD-GRASP: golden-angle radial MRI with reconstruction of extra motion-state dimensions using compressed sensing. Magnetic resonance in medicine. 2016;75(2):775–788. [PubMed: 25809847]
7. Han F, Zhou Z, Han E, et al. Self-gated 4D multiphase, steady-state imaging with contrast enhancement (MUSIC) using rotating cartesian K-space (ROCK): validation in children with congenital heart disease. Magnetic resonance in medicine. 2017;78(2):472–483. [PubMed: 27529745]
8. Pang J, Sharif B, Fan Z, et al. ECG and navigator-free four-dimensional whole-heart coronary MRA for simultaneous visualization of cardiac anatomy and function. Magnetic resonance in medicine. 2014;72(5):1208–1217. [PubMed: 25216287]
9. Di Sopra L, Piccini D, Coppo S, Stuber M, Yerly J. An automated approach to fully self-gated free-running cardiac and respiratory motion-resolved 5D whole-heart MRI. Magn Reson Med. Dec 2019;82(6):2118–2132. [PubMed: 31321816]
10. Rosenzweig S, Scholand N, Holme HCM, Uecker M. Cardiac and Respiratory Self-Gating in Radial MRI Using an Adapted Singular Spectrum Analysis (SSA-FARY). IEEE Trans Med Imaging. Oct 2020;39(10):3029–3041. [PubMed: 32275585]
11. Roy CW, Di Sopra L, Whitehead KK, et al. Free-running cardiac and respiratory motion-resolved 5D whole-heart coronary cardiovascular magnetic resonance angiography in pediatric cardiac patients using ferumoxytol. Journal of Cardiovascular Magnetic Resonance. 2022;24(1):1–12. [PubMed: 34986851]
12. Chia JM, Fischer SE, Wickline SA, Lorenz CH. Performance of QRS detection for cardiac magnetic resonance imaging with a novel vectorcardiographic triggering method. Journal of Magnetic Resonance Imaging. 2000;12(5):678–688. [PubMed: 11050637]
13. Contijoch F, Iyer SK, Pilla JJ, et al. Self-gated MRI of multiple beat morphologies in the presence of arrhythmias. Magnetic resonance in medicine. 2017;78(2):678–688. [PubMed: 27579717]

14. Contijoch F, Rogers K, Rears H, et al. Quantification of left ventricular function with premature ventricular complexes reveals variable hemodynamics. Circulation: Arrhythmia and Electrophysiology. 2016;9(4):e003520. [PubMed: 27009416]
15. Nayak KS, Lim Y, Campbell-Washburn AE, Steeden J. Real-Time Magnetic Resonance Imaging. Journal of Magnetic Resonance Imaging. 2022;55(1):81–99. [PubMed: 33295674]
16. Eirich P, Wech T, Heidenreich JF, et al. Cardiac real-time MRI using a pre-emphasized spiral acquisition based on the gradient system transfer function. Magn Reson Med. May 2021;85(5):2747–2760. [PubMed: 33270942]
17. Yin G, Cui C, An J, et al. Assessment of Left Ventricular Systolic Function by Cardiovascular Magnetic Resonance Compressed Sensing Real-Time Cine Imaging Combined With Area-Length Method in Normal Sinus Rhythm and Atrial Fibrillation. Front Cardiovasc Med. 2022;9:896816. doi:10.3389/fcvm.2022.896816 [PubMed: 35711346]
18. Allen BD, Carr ML, Markl M, et al. Accelerated real-time cardiac MRI using iterative sparse SENSE reconstruction: comparing performance in patients with sinus rhythm and atrial fibrillation. Eur Radiol. Jul 2018;28(7):3088–3096. [PubMed: 29383529]
19. Goebel J, Nensa F, Schemuth HP, et al. Real-time SPARSE-SENSE cine MR imaging in atrial fibrillation: a feasibility study. Acta Radiol. Aug 2017;58(8):922–928. [PubMed: 28273733]
20. Laubrock K, von Loesch T, Steinmetz M, et al. Imaging of arrhythmia: Real-time cardiac magnetic resonance imaging in atrial fibrillation. Eur J Radiol Open. 2022;9:100404. doi:10.1016/j.ejro.2022.100404 [PubMed: 35265735]
21. Derbyshire JA, Saybasili H, Guo L, et al. Golden-step phase encoding for flexible realtime Cardiac MRI. Journal of Cardiovascular Magnetic Resonance. 2011;13(1):1–3. [PubMed: 21208447]
22. Scheffler K, Lehnhardt S. Principles and applications of balanced SSFP techniques. European radiology. 2003;13(11):2409–2418. [PubMed: 12928954]
23. Uecker M, Lai P, Murphy MJ, et al. ESPIRiT—an eigenvalue approach to autocalibrating parallel MRI: where SENSE meets GRAPPA. Magnetic resonance in medicine. 2014;71(3):990–1001. [PubMed: 23649942]
24. Guo L, Herzka DA. Sorted Golden-step phase encoding: an improved Golden-step imaging technique for cardiac and respiratory self-gated cine cardiovascular magnetic resonance imaging. Journal of Cardiovascular Magnetic Resonance. 2019;21(1):1–15. [PubMed: 30612574]
25. Duda RO, Hart PE. Pattern classification and scene analysis. vol 3. Wiley New York; 1973.
26. Lustig M MATLAB code of ESPIRiT. Michael Lustig's software homepage. Accessed November 25, 2020. https://people.eecs.berkeley.edu/~mlustig/Software.html
27. Han F, Rapacchi S, Hu P. Prospective cardiac motion self-gating. Quantitative imaging in medicine and surgery. 2017;7(2):215. [PubMed: 28516047]
28. Caliński T, Harabasz J. A dendrite method for cluster analysis. Communications in Statistics-theory and Methods. 1974;3(1):1–27.
29. Block KT, Uecker M, Frahm J. Undersampled radial MRI with multiple coils. Iterative image reconstruction using a total variation constraint. Magn Reson Med. Jun 2007;57(6):1086–98. [PubMed: 17534903]
30. Heerfordt J, Whitehead KK, Bastiaansen JA, et al. Similarity-driven multi-dimensional binning algorithm (SIMBA) for free-running motion-suppressed whole-heart MRA. Magnetic Resonance in Medicine. 2021;86(1):213–229. [PubMed: 33624348]
31. Uecker M, Zhang S, Voit D, Karaus A, Merboldt KD, Frahm J. Real-time MRI at a resolution of 20 ms. NMR in Biomedicine. 2010;23(8):986–994. [PubMed: 20799371]

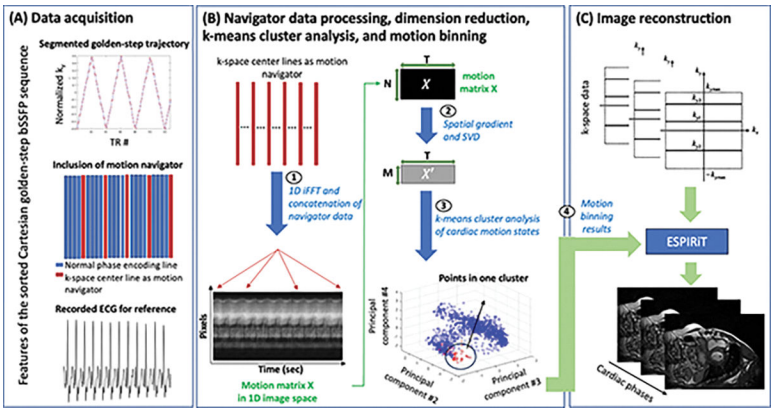

Figure 1.

Overview summary of the proposed cluster-based cine cardiac magnetic resonance framework. (A) Data were acquired using the proposed sorted Cartesian golden-step bSSFP with additional k-space center lines to serve as motion navigators (red bars). ECG signal was recorded for reference. (B) 1D inverse FFT (iFFT) was applied to the navigator k-space center lines and the navigator data were then concatenated to form a motion data matrix X, which is the time series of self-gating projections. Principal component analysis using single value decomposition (SVD) of matrix X was applied to reduce high dimension data from N×T to compressed data X' with M×T (where N>M). Compressed data X' are regarded as T data samples and used as inputs into the cluster algorithm. Outputs are motion binning results with T cluster numbers representing data in one specific cluster. (C) Using ESPIRiT reconstruction, cine images were generated based on sequence trajectory and motion binning results from navigator data processing.

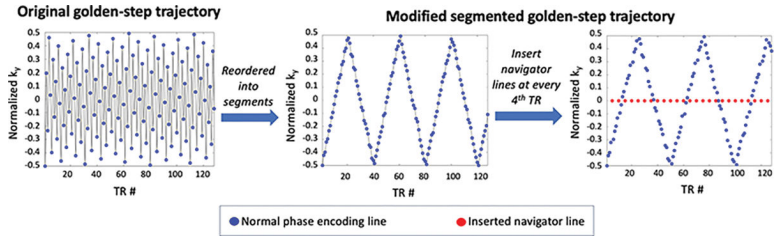

Figure 2.

Modifications of the original golden-step pulse sequence. To create the sorted Cartesian golden-step bSSFP pulse sequence, the original golden-step phase encoding was re-ordered to decrease the gap between adjacent phase encoding lines. There are 20 lines in each segment. The middle image show reordering of the phase encoding lines into segments. The x-axis is the index for phase encoding lines and the y-axis represents locations of the lines in the k_y dimension. The red dots represent k-space navigator lines.

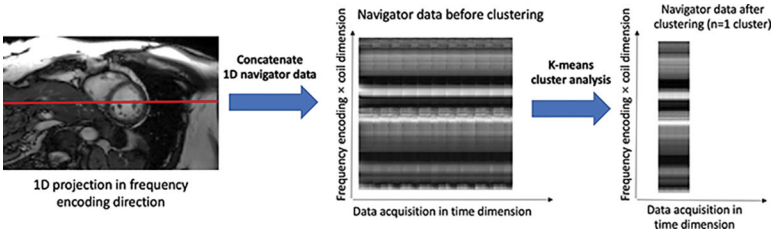

Figure 3.

Navigator data in image space before and after k-means clustering. 1D projections (red line) of navigator data from two coils closest to the heart are concatenated and compressed. Before clustering (middle panel), there were 495 sets of navigator data. After applying k-mean cluster analysis, navigator data from a single sample cluster (right panel) shows sharp alignment, suggesting good performance of the motion clustering algorithm.

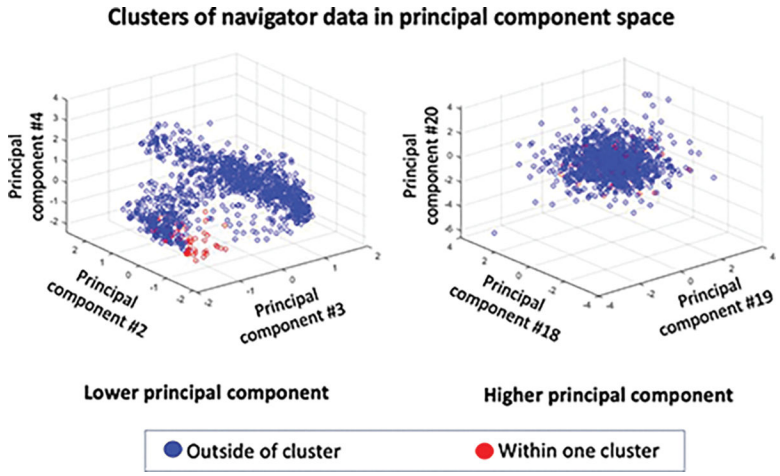

Figure 4.

Data clusters in principal component space. Data within a cluster and outside of a cluster are shown in 3D space using lower principal component dimensions #2, 3, 4 (left) and higher component dimensions #18, 19, 20 (right). In lower principal component dimensions, the whole data distribution deviated from the shape of a sphere or an ellipse; the data within one cluster (red) can be easily distinguished from the data outside of the cluster (blue). In higher principal component dimensions, however, the entire data distribution was closer to an ellipse, reflecting the difficulty of distinguishing data within the cluster and data outside of the cluster because they had similar values.

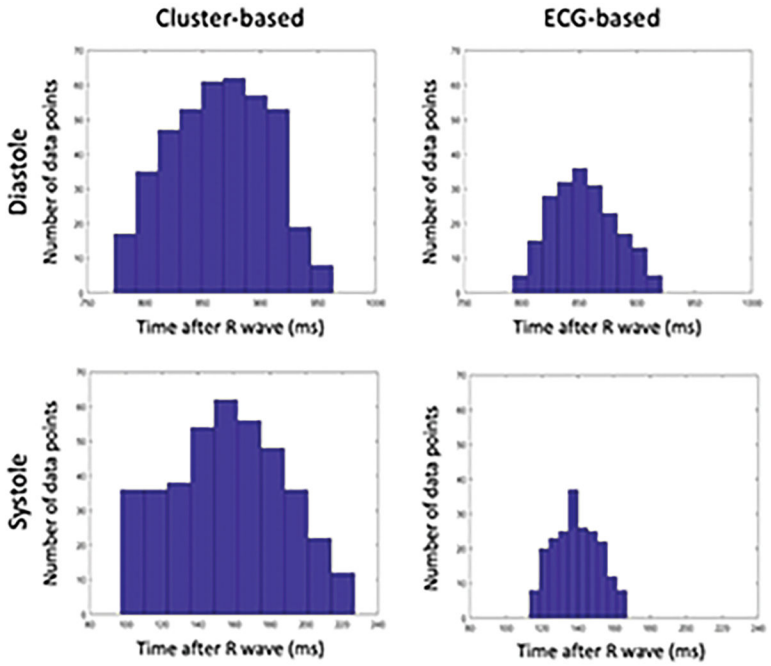

Figure 5.

Distribution of data selection by the proposed cluster-based and ECG-based method within a cardiac cycle from one patient. In each plot, the x-axis represents the time interval after the R-wave and the y-axis represents number of included data points. The cluster-based approach included more data in the end-diastolic and early systolic phases and the distribution is wider within each cardiac cycle.

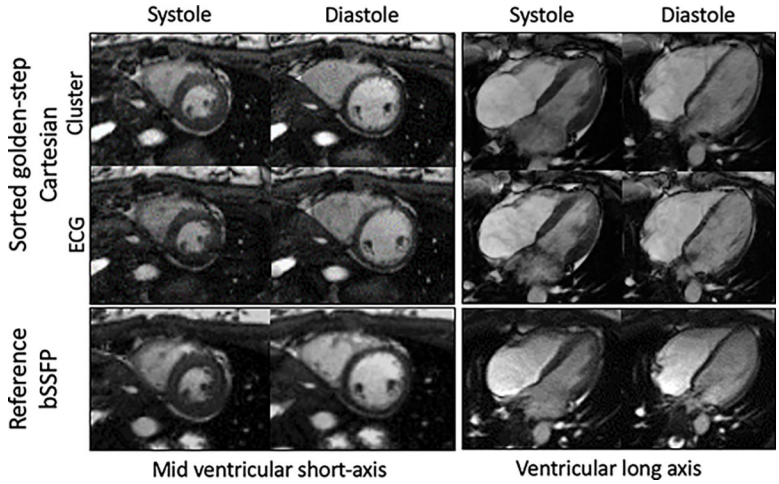

Figure 6.

Representative examples of short and long axis images from one non-contrast scan at 3.0T. The subject was a healthy volunteer (25y, female) with a heart rate of 56 bpm. Images were reconstructed with the cluster-based reconstruction (first row), ECG-based using recorded ECG (second row). The third row consists of images from the reference ECG-gated balanced steady-state free precession (bSSFP) cine sequence. The systolic and diastolic frames from the cluster-based, ECG-based, and reference images all received the highest image quality score (score=4). The overall multiphase image quality scores were 3 vs 3 vs 4 for cluster-based, ECG-based, and reference images, respectively.

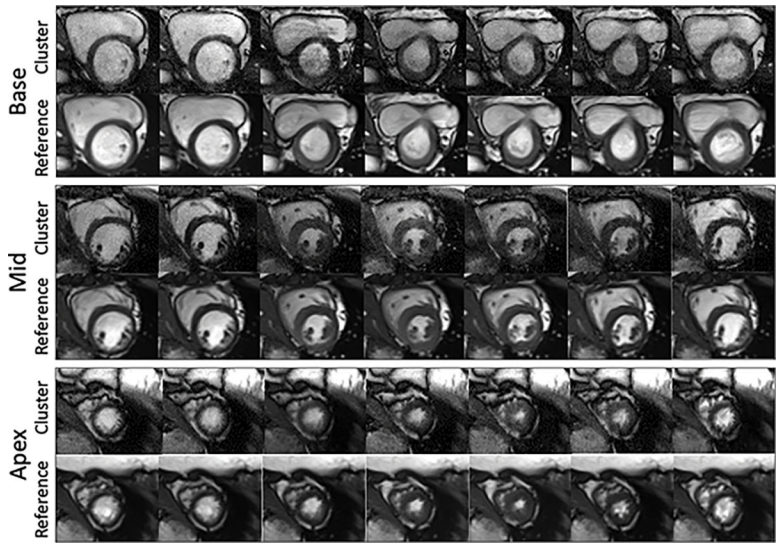

Figure 7.

Ventricular short axis images across several representative phases of the cardiac cycle. Shown are basal, mid ventricular, and apical left ventricular short axis images across seven of 23 frames acquired using the ECG-free sorted Cartesian golden-step cine with cluster-based binning (Cluster) and the ECG-gated reference cine bSSFP sequence with conventional inline reconstruction. The subject was in sinus rhythm. The systolic and diastolic frames from the cluster-based and the reference method both received the highest image quality score (score=4). The overall multiphase image quality scores for the cluster-based method were 3, 4, and 4 for the base, mid, and apical slice respectively, whereas the reference method received a score of 4 for all three slices. A movie file of the images is available as Video S1 (see Supplementary Material). SAX, short axis; bSSFP, balanced steady-state free precession.

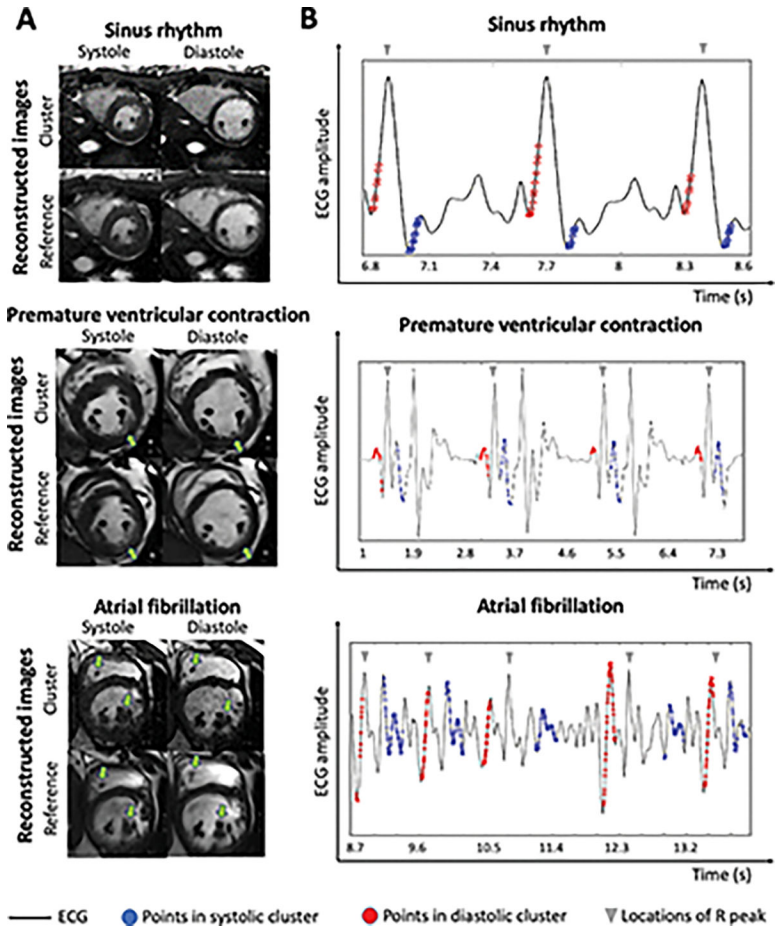

Figure 8.

Comparison of cluster-based and reference cine bSSFP approaches. (A) Early systolic and end-diastolic images acquired in subjects with sinus rhythm and patients with irregular cardiac motion states using the proposed cluster-based and reference methods are shown. Cluster-based images (Cluster) were acquired with the proposed sorted golden-step sequence and reconstructed with the proposed cluster-based reconstruction. Reference images in the second row (Reference) were acquired using the reference bSSFP cine sequence for the patient with sinus rhythm subject and PVC; real-time bSSFP sequence was used as the reference for the patient with atrial fibrillation. Green arrows point to structures that have better conspicuity with the cluster-based relative to the reference reconstructions. (B) Shown are recorded ECG signals in subjects with sinus rhythm, PVCs, and atrial fibrillation. The R peaks are defined by the gray arrowheads. Points chosen by the proposed cluster method are depicted in blue and red. Blue points are binned into the early systolic cluster while red points are binned into the end-diastolic cluster. bSSFP, balanced steady-state free precession; PVC, premature ventricular contraction; SAX, short axis.

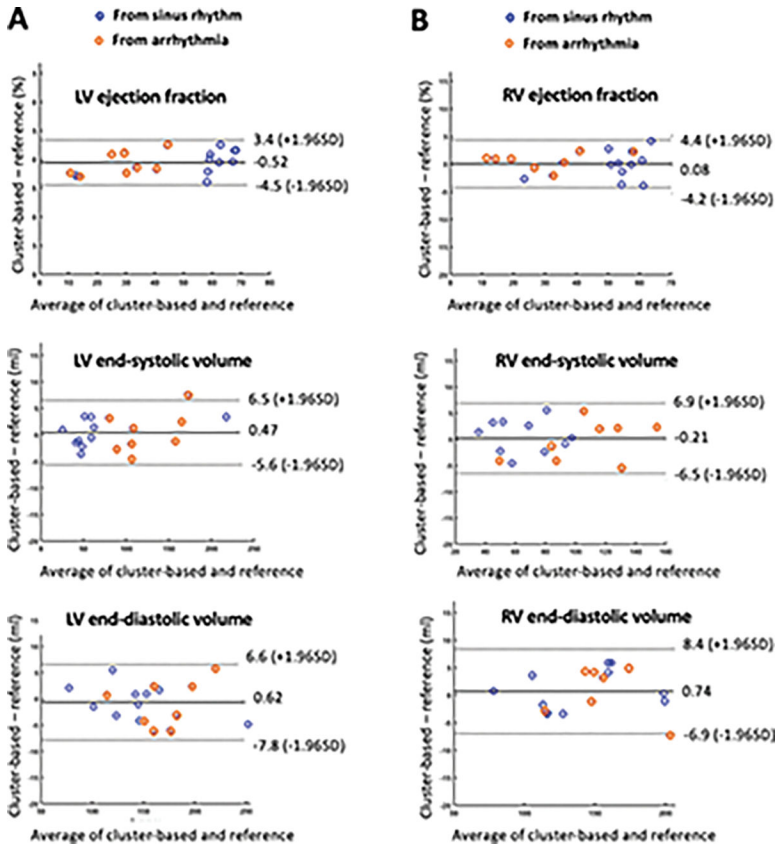

Figure 9.

Bland-Altman plots comparing (A) left ventricular and (B) right ventricular metrics of cardiac function. The metrics are derived from the proposed cluster-based method and reference ECG-gated breath-held cine bSSFP pulse sequence/reference breath-held bSSFP real-time sequence. In the Bland-Altman plots, the dotted horizontal lines represent the 95% limit of agreement. Red points represent data of arrhythmia subjects from cluster-based method vs reference real-time sequence and blue points represent data of sinus rhythm subjects from cluster-based method vs reference bSSFP sequence. Across all metrics of cardiac function, the average bias between the two methods is negligible. See Supplemental Material Figure S2 for correlation plots. bSSFP, balanced steady-state free precession; EF, ejection fraction; EDV, end-diastolic volume; ESV, end-systolic volume; LV, left ventricle; RV, right ventricle.

Table 1.

Representative pulse sequence parameters for sorted Cartesian golden-step bSSFP and reference cine at 3.0 T.

Parameter	Cine bSSFP	Real-time cine bSSFP	Sorted Cartesian golden-step bSSFP
FOV (mm^2)	380*285	380*285	380*285
Spatial resolution (mm^2)	1.8*1.8	1.8*1.8	1.8*1.8
Slice thickness (mm)	8	8	8
Flip angle (degrees)	45–55	45–55	45–55
Asymmetric echo factor	off	off	off
Partial Fourier factor	off	off	off
Parallel acceleration factor	2	off	off
TR (ms)	3.2	3.1	3.4
TE (ms)	1.6	1.5	1.7
Receiver bandwidth (Hz /pixel)	960	957	962
ECG-gating	Yes	No	No
Acquisition time per 2D slice (second)	9–15 (heart rate dependent)	9–20 (depends on arrhythmia rejection)	18 (fixed)

bSSFP, balanced steady-state free precession; ECG, electrocardiogram; FOV, field of view; TE, echo time; TR, repetition time

Table 2.

Comparison of cardiac functional metrics derived from the cluster-based vs reference bSSFP cine MRI at 3.0 T.

Parameter	Mean bias**	Coefficient of variation (%)**	95% Confidence interval*	P value*
LV EF (%)	−0.52	4.5	−1.52 to 0.47	0.28
LV EDV (mL)	−0.62	2.4	−2.45 to 1.21	0.48
LV ESV (mL)	+0.47	3.4	−1.07 to 2.01	0.53
LV mass (mL)	1.20	4.4	−0.84 to 3.30	0.23
RV EF (%)	+0.08	5.2	−1.01 to 1.17	0.88
RV EDV (mL)	0.74	2.7	−1.21 to 2.69	0.44
RV ESV (mL)	0.21	4.1	−1.49 to 1.91	0.80

* Group comparisons using paired t-tests with corresponding 95% confidence intervals.

** Mean bias and coefficients of variation are derived from Bland-Altman analyses. All data points were within the 95% limits of agreement.

EDV, end-diastolic volume; EF, ejection fraction; ESV, end-systolic volume; LV, left ventricular; MRI, magnetic resonance imaging; RV, right ventricular.